Angiogenesis (2015) 18:69–81
DOI 10.1007/s10456-014-9447-0

ORIGINAL PAPER

Contrast-enhanced molecular ultrasound differentiates endoglin genotypes in mouse embryos

J. M. Denbeigh · B. A. Nixon · J. J. Y. Lee · M. Jerkic · P. A. Marsden · M. Letarte · M. C. Puri · F. S. Foster

Received: 5 June 2014 / Accepted: 26 September 2014 / Published online: 9 October 2014

Abstract Targeted ultrasound contrast imaging has the potential to become a reliable molecular imaging tool. A better understanding of the quantitative aspects of molecular ultrasound technology could facilitate the translation of this technique to the clinic for the purposes of assessing vascular pathology and detecting individual response to treatment. The objective of this study was to evaluate whether targeted ultrasound contrast-enhanced imaging can provide a quantitative measure of endogenous biomarkers. Endoglin, an endothelial biomarker involved in the processes of development, vascular homeostasis, and altered in diseases, including hereditary hemorrhagic telangiectasia type 1 and tumor angiogenesis, was the selected target. We used a parallel plate perfusion chamber in which endoglin-targeted (MB_E), rat isotype IgG_2 control and untargeted microbubbles were perfused across endoglin wild-type ($Eng^{+/+}$), heterozygous ($Eng^{+/-}$) and null ($Eng^{-/-}$) embryonic mouse endothelial cells and their adhesion quantified. Microbubble binding was also assessed in late-gestation, isolated living transgenic $Eng^{+/-}$ and $Eng^{+/+}$ embryos. Nonlinear contrast-specific ultrasound imaging performed at 21 MHz was used to collect contrast mean power ratios for all bubble types. Statistically significant differences in microbubble binding were found across genotypes for both in vitro ($p < 0.05$) and embryonic studies ($p < 0.001$); MB_E binding was approximately twofold higher in $Eng^{+/+}$ cells and embryos compared with their $Eng^{+/-}$ counterparts. These results suggest that molecular ultrasound is capable of reliably differentiating between molecular genotypes and relating receptor densities to quantifiable molecular ultrasound levels.

Keywords Micro-ultrasound · Molecular imaging · Mouse embryo · Microbubble contrast agent · Endoglin

Abbreviations

BPM	Beats per minute
CI	Confidence interval
CMPR	Contrast mean power ratio
E	Embryonic day
E:β	Endoglin:β-actin ratio
Eng	Endoglin
$Eng^{+/+}$	Endoglin wild-type
$Eng^{+/-}$	Endoglin heterozygous
$Eng^{-/-}$	Endoglin homozygous null
E:P	Endoglin:PECAM-1 ratio

Electronic supplementary material The online version of this article (doi:10.1007/s10456-014-9447-0) contains supplementary material, which is available to authorized users.

J. M. Denbeigh (✉) · B. A. Nixon · P. A. Marsden · M. C. Puri · F. S. Foster
Department of Medical Biophysics, Sunnybrook Research Institute, Sunnybrook Health Sciences Centre, University of Toronto, 2075 Bayview Avenue, S640, Toronto, Ontario M4N 3M5, Canada
e-mail: janet.denbeigh@utoronto.ca

J. J. Y. Lee · P. A. Marsden
Department of Medicine and Pathobiology, Li Ka Shing Knowledge Institute, St. Michael's Hospital, University of Toronto, Toronto, Ontario M5B 1W8, Canada

M. Jerkic
Anesthesia Research, Keenan Research Centre, St. Michael's Hospital, University of Toronto, Toronto, Ontario M5B 1T8, Canada

M. Jerkic · M. Letarte
Department of Immunology, The Hospital for Sick Children, University of Toronto, Toronto, Ontario M5G 1X8, Canada

M. C. Puri
Lunenfeld-Tanenbaum Research Institute, Mount Sinai Hospital, Toronto, Ontario M5G 1X5, Canada

HR	Heart rate
MB_C	Rat isotype IgG_2 control antibody-targeted microbubbles
MB_E	Endoglin-targeted microbubbles
MB_U	Untargeted microbubbles
MFI	Median fluorescence intensity
ROI	Region of interest
TGFβ	Transforming growth factor β
US	Ultrasound

Introduction

The growing demand for a personalized approach to treatment of vascular disease has accentuated the importance of molecular imaging, defined as the characterization and measurement of key biomolecules in vivo [1]. It has been suggested that molecular ultrasound imaging is one approach that may be used to detect and quantify expression levels of biomarkers on the vascular endothelium [2]. Targeted contrast-enhanced ultrasound imaging has been achieved using small, reflective, oscillating microbubbles (see [3] for a comprehensive review). When decorated with peptides, antibodies, or glycoprotein ligands [4], these bubbles may actively bind to targets associated with angiogenesis, inflammation, thrombi and plaque [5, 6], including vascular endothelial growth factor receptors (VEGFRs) [7], $\alpha_v\beta_3$ integrin [8] and P-selectin [9, 10]. Molecular imaging with ultrasound therefore extends the abilities of a modality that already offers non-ionizing, portable real-time noninvasive imaging with high spatial resolution [11].

There is considerable evidence that targeted microbubbles can be used to detect the presence of various biomarkers in vivo, with the majority of studies suggesting that a positive correlation exists between the magnitude of the molecular ultrasound signal and a measure of the biomarker's expression [12]. They are limited, however, in their ability to say with certainty what portion of the bound bubbles are actually detected and whether the microbubble binding and detection is a consistent and quantitative assessment of molecular expression. The nature of the xenograft model (including variability in tumor hemodynamics [13] and in biomarker expression across different tumor sizes and types [14]) as well as challenges related to biomarker quantification (lack of absolute measures or standardized practices [15–17]) makes it difficult to define the capacity of targeted microbubble imaging to directly quantify biomarker expression levels [2, 18]. This is unfortunate, since quantitative targeted microbubble imaging has the potential to dramatically impact all facets of patient care, from early disease detection and classification [19] to diagnosis, staging, individualized treatment monitoring and day-to-day management of patients [20].

Our objective was to determine whether molecular ultrasound could provide a quantitative measure of vascular biomarker expression. Direct modulation of surface target protein densities within a model system that allows distinct comparison and correlation between in vitro and in vivo endothelial binding was desirable. The implementation of an embryonic loss of function model addressed this need. Genetic manipulations can generate heterozygous (+/−) and homozygous null (−/−) mice and cultured endothelial cells for various vascular biomarkers including $\alpha_2\beta_1$ integrin [21], P-selectin [22], and endoglin [23]. What is more, the mouse embryo exhibits highly regulated and controlled angiogenesis during development, in contrast to the heterogeneous patterns of the tumor microenvironment. This makes them highly suitable for examining whether molecular ultrasound can be used to quantitatively differentiate between molecular genotypes and related receptor densities. What is more, the feasibility of microbubble imaging within mouse embryos has been previously established [24, 25], and molecular imaging of endogenously expressed endothelial cell surface markers in the developing mouse embryo is possible [26].

An endoglin loss of function model was selected to test whether targeted microbubble binding could differentiate between genotype groups. Originally characterized over two decades ago [27], endoglin is a major transmembrane glycoprotein predominantly expressed on proliferating endothelial cells [28] and it acts as a co-receptor for several members of the transforming growth factor β (TGFβ) superfamily [29]. It plays a key role in biological processes including developmental angiogenesis and vasculogenesis, modulation of vascular tone in response to hemodynamic stress [30] and response of tissue to hypoxia [31, 32]. In addition, endoglin is recognized as a marker of disease; it is mutated in hereditary hemorrhagic telangiectasia type 1 (HHT1) [33], with haploinsufficiency as the underlying cause of disease. An excess of placental endoglin and circulating soluble endoglin is associated with pre-eclampsia [34], while increased endoglin on tumor vessels is a marker of tumor angiogenesis [35]. Endoglin is thus a promising target for anti-angiogenic therapies, with endoglin-Fc constructs, endoglin vaccines and endoglin-neutralizing antibodies [28] currently undergoing evaluation. Endoglin has also attracted attention as a viable target for molecular ultrasound. Korpanty et al. first used an avidin-/biotin-linking system to attach monoclonal antibodies against mouse endoglin (MJ7/18) to microbubbles and demonstrated specific binding to endothelial cells under static conditions [36, 37]. More recently, Willmann et al. [2] assessed the ability of endoglin-targeted

microbubbles to bind to cultured tumor cells and to differentiate between tumors in mice with low versus high endoglin expression levels.

Therefore, the purpose of this study was to evaluate whether targeted contrast-enhanced ultrasound provides a noninvasive measure of endothelial biomarker expression in our endoglin model. Our hypothesis was tested using a parallel plate perfusion chamber to mimic the normal physiology of blood flow. Endoglin-targeted microbubbles were perfused across embryonic mouse endothelial cells [endoglin wild-type ($Eng^{+/+}$), heterozygous ($Eng^{+/-}$) and homozygous null ($Eng^{-/-}$)] and their adhesion quantified. We also measured the binding of endoglin-targeted microbubbles in isolated late-gestation living transgenic endoglin embryos ($Eng^{+/+}$ and $Eng^{+/-}$). Our results suggest that targeted microbubble binding does indeed provide a measure of endoglin expression on endothelial cells, both in vitro and in vivo, relating receptor densities to quantifiable molecular ultrasound levels. With further refinement and clinical validation, endoglin-targeted contrast imaging may someday serve as a powerful tool for assessing the efficacy of inhibiting drugs, monitoring treatment response and dose optimization in individuals [38] or providing a measure of a tumor's metastatic potential [39].

Methods and data analysis

Expanded methods, and details regarding the analysis pipeline, are available in the online-only Supplemental Materials.

Mouse embryonic endothelial cells

Wild-type ($Eng^{+/+}$), heterozygous ($Eng^{+/-}$) and homozygous null ($Eng^{-/-}$) endothelial cells were cultured and maintained as described previously [40]. The presence (or absence) of endoglin on the surface of each cell type was confirmed by flow cytometry, as detailed in supplemental materials.

Animals

The experimental procedures performed in this study were approved by the Animal Care Committee at Sunnybrook Research Institute (Toronto, ON, Canada). $Eng^{+/-}$ mice were generated by homologous recombination using embryonic stem cells of 129/Ola origin as described by Bourdeau et al. [23]. B6-$Eng^{+/-}$ mice were backcrossed to the CD-1 background (Charles River Laboratories, St-Constant, Quebec, Canada). F9 and F10 generations of $Eng^{+/-}$ CD-1-backcrossed embryos were used, as well as their $Eng^{+/+}$ littermate controls. Genotypes were determined by standard PCR analysis [41] (see supplemental materials). Embryos were removed at gestational embryonic days (E) 16.5 and E17.5, with E0.5 defined as noon of the day a vaginal plug was observed.

Microbubble preparation

MicroMarker targeting microbubbles (VisualSonics. Inc., Toronto, ON) were reconstituted from a freeze-dry powder with saline. Three types of microbubbles were prepared: endoglin-targeted microbubbles (MB_E); rat isotype IgG_2 control antibody-targeted microbubbles (MB_C); and untargeted microbubbles (MB_U). One milliliter of PBS was slowly injected into a microbubble vial using a 21-G needle; the plunger was withdrawn, removing 1 mL of air, and the needle was removed; the vial was gently agitated and left to stand 5 min. Biotinylated rat MJ 7/18 antibody to mouse endoglin and rat isotype IgG_2 control-targeting mouse IgG2a (Biotin, eBioscience) were coupled to the lipid-shelled, perfluorocarbon-containing microbubbles through streptavidin (bubble)—biotin (antibody) interactions via the addition of 20 μg (recommended by MicroMarker) of antibody in 1 mL saline (final volume). The final mixture (2 mL) was left to stand for 10 min. Assuming complete surface conjugation, the average number of bound ligand for the microbubbles was approximately [42] 7,600 ligands/μm^2. In a subset of cases, 0.5 mL of streptavidin magnetic beads (New England BioLabs, Whitby, ON, Canada, 4 mg/mL) was added to the vial for 5 min to bind excess biotinylated antibody. The beads were separated from the microbubble solution with a magnet prior to counting and use. Untargeted microbubbles, without streptavidin, were also reconstituted with 2 mL saline. The concentration and size distribution of the microbubble vials were quantified using a Beckman Coulter Counter (Multisizer 3, Beckman Coulter Canada Inc., Mississauga, ON, Canada).

Parallel plate flow chamber studies

Targeted microbubble adhesion of MB_E, MB_C and MB_U microbubbles under flow shear stress conditions to $Eng^{+/+}$, $Eng^{+/-}$ and $Eng^{-/-}$ endothelial cells was assessed in vitro using a flow chamber experimental setup, as detailed in supplemental materials. Refer to Fig. 1a and Online Resource Fig. 1.

Injection of microbubbles into embryos

Preparations for ultrasound molecular imaging were performed as previously described [26] and detailed in supplemental materials.

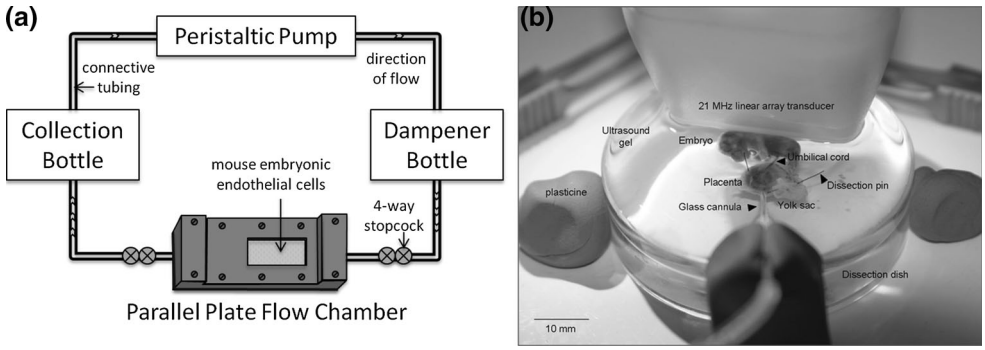

Fig. 1 **a** Schematic of parallel plate flow chamber experimental setup. Endoglin wild-type ($Eng^{+/+}$), heterozygous ($Eng^{+/-}$) and null ($Eng^{-/-}$) mouse embryonic endothelial cells were cultured on glass slides and mounted in parallel plate flow chambers. Microbubbles (endoglin-targeted: MB_E, isotype control: MB_C or untargeted: MB_U) were diluted at 1×10^7 MB/mL in PBS in the dampener bottle and perfused across the cells at 4 mL/min, corresponding to a shear stress of approximately 2 dynes/cm^2. **b** Experimental setup for the injection of microbubbles into isolated embryos. With permission from Denbeigh et al. [26]. A 21 MHz linear array transducer (Vevo2100) is positioned above an exteriorized living E16.5 embryo as 20 μL microbubble solution is injected into a placental vein using a glass cannula. *Scale bar* = 10 mm

Surgical procedure

The surgical procedures performed in this study, adapted from Whiteley et al. [43], were approved by the Animal Care Committee at Sunnybrook Research Institute (Toronto, ON, Canada). Embryos were removed at gestational days E16.5–E17.5. The pregnant mouse was sacrificed by cervical dislocation and the uterus was removed and placed immediately in chilled embryo media. The uterus was then transferred to a culture dish filled with fresh chilled embryo media. The embryos were dissected out with forceps, keeping the yolk sacs intact and handling the placenta gently. A perforated spoon was used to move the embryos, which were kept on ice with fresh media (changed every 1–1.5 h).

Injection of microbubbles into embryos

Each embryo was injected once with a single-bubble type. The genetic identity of each embryo was unknown prior to injection and quantification of molecular signal. After random selection, the embryo was placed in a dissection dish, gently removed from within the yolk sac, pinned in place and washed with pre-warmed PBS (maintained in a water bath at 45 °C [43]). After revival, the umbilical vein and associated vessels were identified, with visible pumping of blood in the umbilical artery and bright red blood initially filling the veins. In general, branches arising from the umbilical vein usually overlay those from the umbilical artery. Pre-warmed ultrasound gel was used to cover and surround the embryo, and this was topped with warm PBS to fill the dish. The glass needle was mounted on a plasticine base and inserted into the PBS. A placental vein on the chorionic surface of the placental disc was selected for injection, and the tip of the needle was trimmed to size (diameter 50–100 μm) with Vannas-Tubingen scissors (Fine Science Tools, North Vancouver, BC, Canada). Microbubble solution was injected with the pump at 20 μL/min with a syringe infusion pump (Bio-lynx NE-1000, New Era Pump Systems Inc., Farmingdale, NY) through the needle until all of the air was expelled from the tip and microbubbles were observed to flow freely. The pump was stopped and reset for an injection volume of 20 μL. The glass needle was gently inserted into the desired vessel and fixed in place for the entire imaging experiment. The transducer was immediately positioned above the embryo, and 20 μL of microbubble solution was injected at 20 μL/min using the syringe pump. See Fig. 1b. Ultrasound imaging was then initiated. Post injection, embryos were euthanized via decapitation, tail samples were taken for PCR genotyping, and the skull was cut in half with a scalpel. The brain hemispheres were removed, frozen in liquid nitrogen and stored at −80 °C for use in Western blot analysis. For each subsequent embryo injection, a fresh dissection dish, needle, syringe and tubing segment were used, with preparation of the next batch of microbubble injection solution taking place during dissection and revival.

Ultrasound molecular imaging

Ultrasound imaging of the embryos (see Online Resources Fig. 2), was performed on a Vevo-2100 scanner (VisualSonics Inc.) using a 21 MHz linear array transducer (MS250s, VisualSonics Inc.). All time-gain-compensation sliders were shifted to the exact middle position. Split

screen B-mode and nonlinear contrast-specific mode (standard settings) were employed, using the following parameters: 18 MHz frequency; lateral and axial resolution of 165 and 75 μm, respectively; 4 % transmit power (0.39 MPa); 30 dB contrast gain; 8 mm foci; and wide beam width, with destruction pulses at 100 % transmit power for 0.1 s. To assess targeted microbubble binding during embryonic molecular imaging studies ($n_{+/+} = 68$, $n_{+/-} = 70$), microbubbles were allowed to circulate and adhere for 3 min and 40 s post injection, after which ultrasound imaging was initiated and a 'pre-destruction' acoustic response sequence was recorded at 29 Hz. At 4 min post injection [2, 44], a short burst of high acoustic pressure was employed, destroying all of the microbubbles in the imaging plane. The subsequent 'post-destruction' imaging sequence was assumed to contain only circulating bubble signals that had replenished the beam.

The ratio of the average signal intensity of the 'pre-destruction' to 'post-destruction' sequences was used to produce a measure of the molecular signal called the contrast mean power ratio (CMPR) for each embryo. A linear mixed model was conducted to assess whether significant differences between average MB_E, MB_C and MB_U CMPRs were observed within the brains of $Eng^{+/+}$ and $Eng^{+/-}$ embryos. The estimated CMPR means [mean ± 95 % confidence interval (CI)] are presented for each microbubble and embryo type. Bonferroni adjustments were made for multiple comparisons. Embryos were excluded from analysis if there was profuse bleeding during injection.

Western blotting

Methods used to obtain cell and tissue proteins have been described previously [41, 45]. Standard Western blot methods were used and are described in Supplemental Materials.

Data analysis

Normality was tested using Shapiro–Wilks and equality of variance tested using Levene's F test. Statistical tests (see supplemental materials for full details) were performed in PASW Statistics 18 (IBM Corporation, Armonk, NY, USA), and results were presented with Origin 9 (Northampton, MA, USA). A two-sided p value of <0.05 was considered statistically significant.

Results

We investigated whether contrast-enhanced molecular ultrasound imaging could be used to quantitatively evaluate the expression of endoglin. This hypothesis was tested in vitro on cultured mouse embryonic endothelial cells using a parallel plate flow chamber system and in living, isolated transgenic mouse embryos.

Expression of endoglin in mouse embryonic endothelial cells by Western blotting and flow cytometry

Three types of mouse embryonic endothelial cells were cultured at equivalent densities: $Eng^{+/+}$, $Eng^{+/-}$ and $Eng^{-/-}$. Cellular adhesion, locomotion and morphology differed across genotypes, as reported previously [40, 45]. Differences in endoglin expression levels were confirmed using Western blotting and flow cytometry. Western blot analysis revealed reduced relative amounts of endoglin in the heterozygous cell population, with null expression observed in the $Eng^{-/-}$ cells compared to the wild-type $Eng^{+/+}$ cells, as shown in Fig. 2a. Statistical analysis of the endoglin:β-actin and endoglin:PECAM-1 densitometry ratios ($E{:}\beta^{+/+}_{Eng} = 1.00 \pm 0.10$, $E{:}\beta^{+/-}_{Eng} = 0.71 \pm 0.11$, $E{:}\beta^{-/-}_{Eng} = 0.31 \pm 0.06$ and $E{:}P^{+/+}_{Eng} = 1.00 \pm 0.02$, $E{:}P^{+/-}_{Eng} = 0.46 \pm 0.08$, $E{:}P^{-/-}_{Eng} = 0.29 \pm 0.05$, see Fig. 2b) revealed significant differences ($p < 0.05$) between all genotypes.

These findings were confirmed using flow cytometry, whereby endoglin was present on the $Eng^{+/+}$ (geometric median fluorescence intensity, MFI = 1676), to a lesser extent on $Eng^{+/-}$ cells (MFI = 846), and absent on $Eng^{-/-}$ cells (244, see Fig. 2c). The fluorescence intensity of endoglin + cells was normally distributed, implying variability of expression levels within each population. MFI was found to be 301, 405 and 248 for rat isotype control antibody to $Eng^{+/+}$, $Eng^{+/-}$ and $Eng^{-/-}$ cells, respectively (Fig. 2d).

Expression of endoglin in murine embryos

The second objective was to verify the predicted endoglin profiles for wild-type and heterozygous mouse embryos using Western blot analysis (Fig. 3a). The brain is an ideal target for our microbubble studies due to minimal tissue motion, the presence of regular vascularity compared with more complicated networks found elsewhere (e.g. liver) and the potential for reproducibility in ultrasound probe placement and imaging plane selection. Angiogenesis is also highly active at this phase of neuronal development [46], resulting in the up-regulation of endoglin. Statistical analysis of densitometry ratios acquired from embryonic samples for endoglin:β-actin ($E{:}\beta^{+/+}_{Eng}$: 1.00 ± 0.40 and $E{:}\beta^{+/-}_{Eng}$: 0.59 ± 0.32) and endoglin:PECAM-1 ($E{:}P^{+/+}_{Eng}$: 1.00 ± 0.33 and $E{:}P^{+/-}_{Eng}$: 0.57 ± 0.30) revealed significant reductions ($p < 0.05$) of relative endoglin expression in embryonic heterozygous embryos as shown in Fig. 3b. Endoglin content in brains from $Eng^{+/-}$ embryos is about

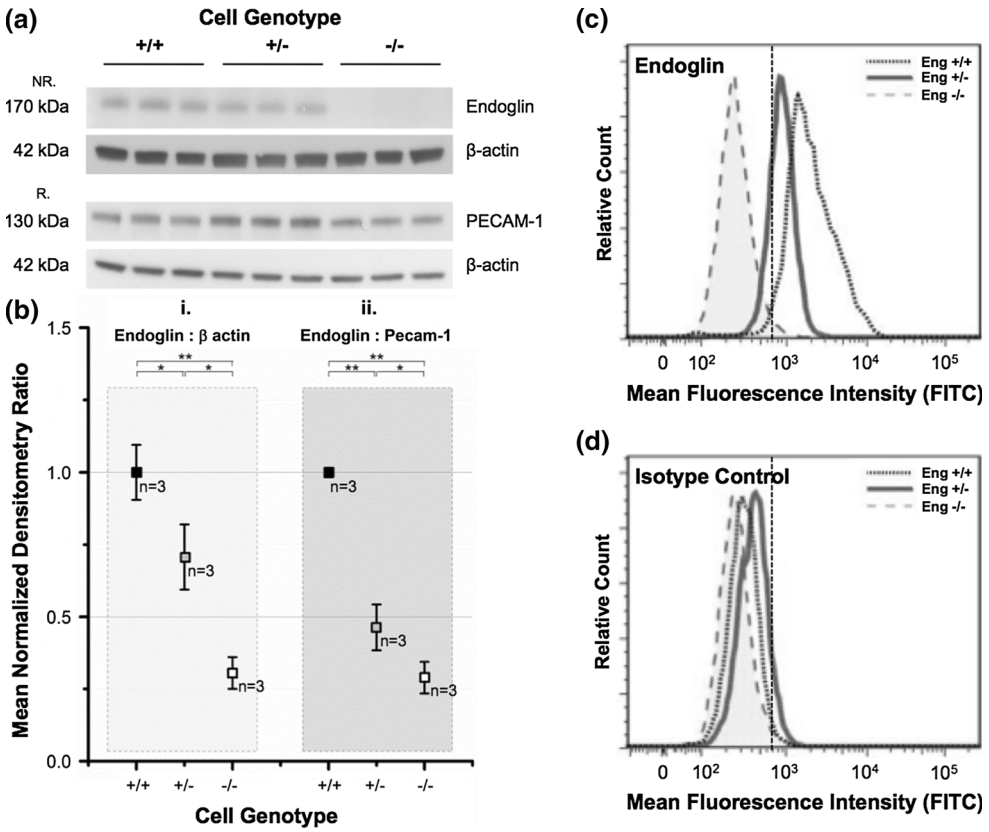

Fig. 2 Endoglin expression in $Eng^{+/+}$, $Eng^{+/-}$ and $Eng^{-/-}$ mouse embryonic endothelial cells (MEEC). **a** Western blot for endoglin expression in $Eng^{+/+}$, $Eng^{+/-}$ and $Eng^{-/-}$ MEEC. Mouse embryonic endothelial cell extracts were fractionated and immunoblotted with antibodies to mouse endoglin [170 kDa dimer under non-reducing conditions (NR)], PECAM-1 [130 kDa, under reducing conditions (R)] and β-actin (42 kDa, reducing and non-reducing conditions). **b** Mean-normalized densitometry ratios in $Eng^{+/+}$, $Eng^{+/-}$, and $Eng^{-/-}$ MEEC. (*i*) Endoglin:β-actin ratios were normalized to $Eng^{+/+}$ mouse endothelial cells; (*ii*) Endoglin:PECAM-1 ratios were normalized to $Eng^{+/+}$ mouse endothelial cells. Endoglin expression was found to significantly decrease across genotypes. Results presented as mean ± S.D. **c**, **d** Flow cytometry analysis of $Eng^{+/+}$, $Eng^{+/-}$ and $Eng^{-/-}$ MEEC. Each cell line was incubated with biotinylated antibodies to endoglin (**c**) or isotype control IgG (**d**) followed by FITC-conjugated streptavidin. Endoglin was present on $Eng^{+/+}$ cells, with a marked reduction in expression for heterozygous $Eng^{+/-}$ cells. Endoglin null cells did not show detectable fluorescence. Results presented as mean ± SD. $^{*}p < 0.05$, $^{**}p < 0.01$

half of that found in $Eng^{+/+}$ littermates, confirming $Eng^{+/-}$ haploinsufficiency.

Microbubble attachment in parallel plate flow chamber studies

To evaluate specific targeting of mouse embryonic endothelial cells with US contrasts agents, we first analyzed the ability of antibody-directed MBs to bind endothelial surfaces under flow conditions. These conditions were selected according to in vivo estimates and parameters detailed in the existing literature [2, 7, 10, 15, 47–49] and the constraints of the experimental set-up. Reconstitution of microbubbles (for both in vitro and embryo experiments) produced an average vial concentration of $3.81 \pm 0.82 \times 10^8$ MB/mL with an average diameter of 1.73 ± 0.16 μm. In an initial pilot study, vials were incubated with ($MB_{E:Beads}$, $n = 2$) and without magnetic sorting beads (MB_E, $n = 2$) to evaluate whether the possible presence of excess unbound biotinylated antibody impacted microbubble binding. Endoglin-targeted binding to $Eng^{+/+}$ cells was not significantly different between vials (data not shown). As a result, subsequent preparations of microbubbles (for all data shown) did not include magnetic bead sorting.

A window feature in the flow chambers made it possible to observe bubble behavior as the microbubble solution moved across a confluent monolayer of cells during perfusion. Following rinsing, bound bubbles remained in the cellular plane of view while free bubbles drifted out of focus. Although bubbles could often be detected in phase imaging (Fig. 4a), better precision for counting was achieved using bright field imaging (Fig. 4b). Overall, very little adherence of untargeted microbubbles was observed ($Eng^{+/+}_{median} = 0.01$ MB_U/cell; $Eng^{+/-}_{median} = 0.01$ MB_U/cell;

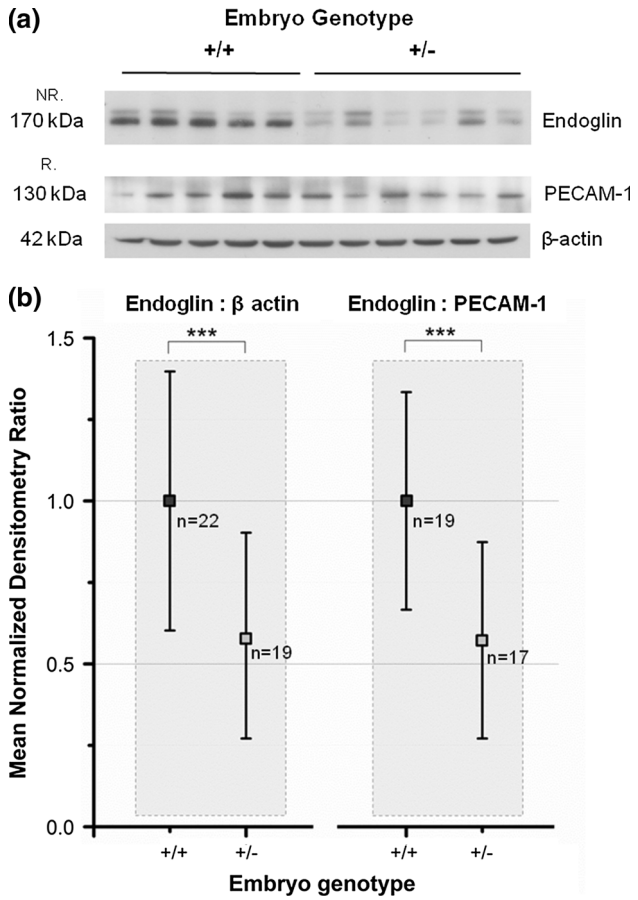

Fig. 3 Endoglin expression in embryonic mouse brains. **a** Western blots for endoglin expression in mouse embryo E17.5 brains. Extracts of brain tissue from E17.5 wild-type ($Eng^{+/+}$) and heterozygous ($Eng^{+/-}$) embryos were fractionated and immunoblotted with antibodies to mouse endoglin [170 kDa non-reducing (NR) conditions], PECAM-1 [130 kDa, reducing (R) conditions] and β-actin (42 kDa, reducing conditions). **b** Mean-normalized densitometry ratios in $Eng^{+/+}$ and $Eng^{+/-}$ embryonic mouse brains. (*i*) Endoglin:β-actin ratios were normalized to $Eng^{+/+}$ mouse embryos; (*ii*) Endoglin:PECAM-1 ratios were normalized to $Eng^{+/+}$ mouse embryos. Endoglin expression was reduced by approximately half in $Eng^{+/-}$ embryos. Results presented as mean ± SD. ***$p < 0.001$

$Eng^{-/-}_{median} = 0.02$ MB_U/cell) with no significant differences across cell genotypes. Adherence of MB_E, however, did differ significantly across MEEC genotypes ($p \leq 0.002$). Endoglin-targeted microbubble binding to $Eng^{+/+}$ cells (median = 0.96 MB_E/cell) was evenly distributed across the entire slide. MB_E were similarly dispersed across $Eng^{-/-}$ cells, although in reduced numbers (median = 0.19 MB_E/cell). Conversely, $Eng^{+/-}$ cells (median = 0.40 MB_E/cell) exhibited MB_E binding in pockets, with bubbles clustered non-uniformly across the cells. In the final group, MB_C binding was highly variable, resulting in significant differences between genotypes ($p \leq 0.003$). While $Eng^{+/+}$ and $Eng^{-/-}$ levels of MB_C binding were reduced compared to MB_E ($Eng^{+/+}_{median} = 0.06$ MB_C/cell; $Eng^{-/-}_{median} = 0.10$ MB_C/cell), a higher proportion of control bubbles were found to bind to $Eng^{+/-}$ cells (median = 0.26 MB_C/cell). These results are summarized in Fig. 4c (and Online Resources Table 1).

Molecular ultrasound imaging in murine embryos

The quantitative nature of molecular ultrasound contrast imaging was further tested in a transgenic embryo model. We assessed whether there was a significant difference in binding signal across varying endoglin expression levels using MB_E, MB_C and MB_U microbubbles. Binding was measured in fourteen separate litters (average number of embryos per litter: 10 ± 2) of mice at embryonic stages E16.5 and E17.5, consisting of wild-type $Eng^{+/+}$ and heterozygous $Eng^{+/-}$ embryos. All embryos were consistently revived within a minute of warming up to 4 h after initial isolation with chilling. The average heart rate (HR) during molecular imaging was found to be 57 ± 14 beats per minute (bpm). Genotype could not be predicted by direct observation of embryos after removal from the uterus, as there was no apparent difference in embryo size or measurable heart rate ($HR^{+/+} = 57 \pm 13$ bpm vs. $HR^{+/-} = 57 \pm 16$ bpm). Moreover, we did not observe a noticeable difference in fragility of vessels or ease of injection between groups.

Nonlinear contrast-enhanced ultrasound imaging confirmed the presence of microbubbles within the entire embryo following a rapid wash-in of the contrast agent. The lateral and axial resolution of the ultrasound images were 165 and 75 μm, respectively. The magnitude of the echogenicity of microbubbles is such that even a single bubble can be detected [50–52]. Imaging signals were collected, and the average CMPR across brain hemispheres were computed for all embryos (Fig. 5, plotted as mean ± 95 % CI). Estimates of the means for fixed effects in the linear mixed model result in genotype, microbubble and the interaction of genotype with microbubble (genotype × microbubble) being the only significant predictors of CMPR (see Online Resources Table 2). For endoglin expression quantification, MB_E binding was found to be nearly twofold higher ($p < 0.001$) in $Eng^{+/+}$ embryos compared with $Eng^{+/-}$ embryos. Furthermore, targeted MB_E binding was significantly ($p < 0.001$) greater than all cases of MB_C and MB_U binding (which were not found to be significantly different ($p = 0.705$) from each other, regardless of embryo genotype).

Discussion

Molecular contrast-enhanced ultrasound imaging is recognized as a useful technique for imaging intravascular

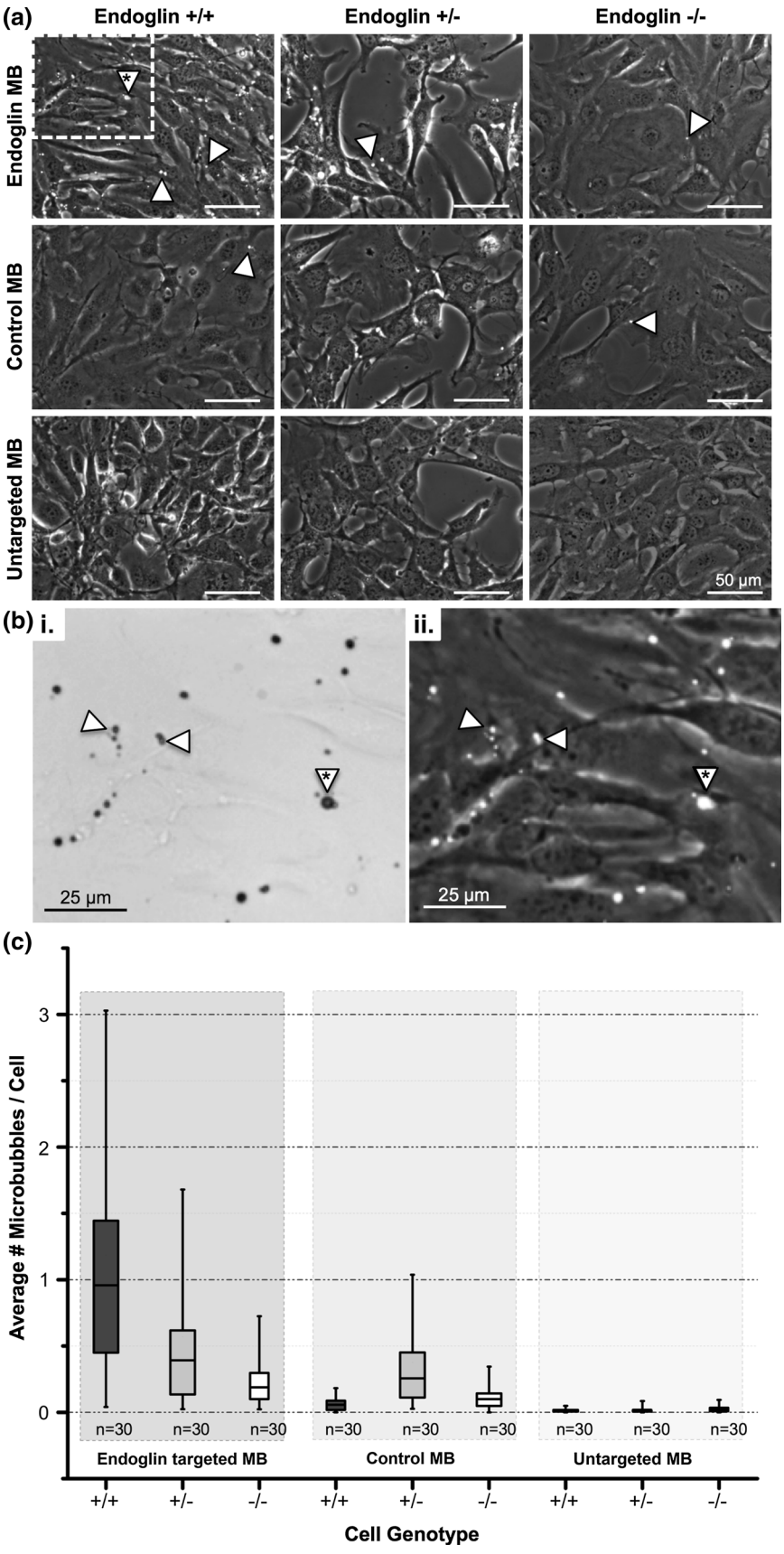

Fig. 4 Microbubble attachment to mouse embryonic endothelial cells. **a** Representative phase images of wild-type ($Eng^{+/+}$), heterozygous ($Eng^{+/-}$) and null ($Eng^{-/-}$) endoglin cells exposed to endoglin-targeted (MB_E), control (MB_C) and untargeted microbubbles (MB_U) under flow shear stress conditions of 2 dynes/cm^2 in flow chamber cell culture attachment studies. Microbubbles can be identified as *small*, *white spheres* (*arrowheads*) in phase contrast images (×40). Binding of MB_E was substantially higher to endoglin-expressing versus null cells. There was minimal attachment of MB_C and MB_U to all cell types. Scale bar = 50 µm. **b** Enlarged view of $Eng^{+/+}$ cells with adherent MB_E. $Eng^{+/+}$ cells (*inset* from (**a**), *dotted line*) under bright field (*i*) and phase (*ii*) illumination showing MB_E attachment. *Scale bar* = 25 µm. *Arrowhead with asterisk* identifies same bubble across all images **c** Quantitative data of endoglin-targeted (MB_E), control (MB_C) and untargeted microbubble (MB_U) binding to $Eng^{+/+}$, $Eng^{+/-}$ and $Eng^{-/-}$ mouse embryonic endothelial cells. *Box* and *whisker plot* (Min., Quartile 1, Median, Quartile 3, Max.) of the average number of attached MBs per cell after 5 min of flow at 4 mL/min. Cell and bubble numbers determined from bright field and phase images (See Fig. 4a, b), with each condition performed in triplicate

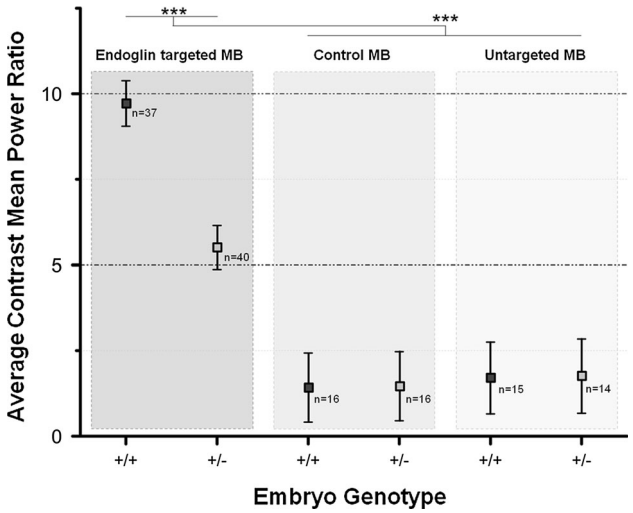

Fig. 5 Summary of the average contrast mean power ratios (CMPR) obtained by molecular ultrasound imaging for endoglin-targeted (MB_E), control (MB_C) and untargeted microbubbles (MB_U) in $Eng^{+/+}$ and $Eng^{+/-}$ embryos. CMPRs from endoglin-targeted microbubbles were significantly higher ($***p < 0.001$) than those collected for MB_C and MB_U, (not significantly different from each other, regardless of genotype). MB_E binding was found to be significantly higher in $Eng^{+/+}$ embryos compared with $Eng^{+/-}$ embryos. Results presented as mean ± 95 % confidence interval

markers in angiogenesis, having repeatedly demonstrated that retention of targeted microbubbles, and thus the signal intensity of the ultrasound images, reflects the presence of target biomarkers [53]. Quantitative correlation between target expression levels in vivo and noninvasive imaging data, however, has not been extensively validated [54]. Further effort is required to understand the quantitative aspects of targeted microbubble imaging in order to facilitate its clinical application for the purposes of assessing vascular pathology and detecting response to treatment. The development of models that permit reproducible control of cell surface target protein densities is required to achieve this goal [55]. In this study, we evaluated whether targeted ultrasound contrast agents could provide a quantitative, noninvasive measure of endoglin expression on endothelial cells.

Traditionally, MB studies have used different tumor cell lines to verify targeted binding to overexpressed receptors present in diseased tissue (and face complications related to variation in yield, growth, flow conditions and expression patterns [55]). In reality, however, in vivo binding is restricted to endothelial cells. Therefore, in this work, we focused on the use of a loss of function model wherein changes in genotype produced variable levels of endoglin expression in both cultured endothelial cells ($Eng^{+/+}$, $Eng^{+/-}$, $Eng^{-/-}$) and murine embryos ($Eng^{+/+}$, $Eng^{+/-}$). This allowed us to directly compare in vitro and in vivo binding results.

Our first objective was to validate the model system. Western blots and flow cytometry revealed little to no detectable expression of endoglin in endoglin null cells ($Eng^{-/-}$) and positive expression for $Eng^{+/+}$ cells, as previously characterized [40]. Likewise, endoglin levels appear to be reduced by approximately half in heterozygous tissue, compared to their $Eng^{+/+}$ counterparts, as expected [56]. For all cases of positively expressing cells, the wide degree of variability in endoglin expression at the cellular level suggests that for quantification purposes, we must consider each population as a whole, rather than individual cells. Within the embryonic brain, a similar trend was observed, with mean-normalized densitometry ratios for endoglin expression reduced by approximately half in $Eng^{+/-}$ samples when compared to normalized $Eng^{+/+}$ samples. The models are thus comparable and demonstrate reproducible differences in endoglin levels.

Our second objective was to assess whether we could achieve specific binding of endoglin-targeted microbubbles to cultured, endoglin-expressing mouse embryonic endothelial cells under physiologically relevant flow conditions and whether the incidence of microbubble adhesion would decrease significantly with reductions in endoglin expression. We employed parallel plate flow chambers, which are used to investigate the fluid shear rates, particle size, concentration and ligand and target site density requirements for promoting microbubble adhesion [9, 42, 57–62]. Flow experiments initially conducted with microbubbles suspended in cell media demonstrated that microbubble binding was almost completely inhibited under this condition, likely due to media blocking microbubble-conjugated antibodies. Early trials also incorporated the use of magnetic beads as a means of removing excess biotinylated antibodies, as previously described [42]. We elected not to pursue this method after finding no significant differences in binding between treated and untreated vials of MB_E to $Eng^{+/+}$ cells. Since microbubble clumping appeared in areas where cells were not confluent we also experimented with alternate substrates. We observed no significant differences in MB_E attachment across $Eng^{+/+}$ cells grown on glass slides with 0.1 % gelatin, 0.1 % fibronectin or substrate free (data not shown), suggesting that cell substrates do not influence bubble binding.

Selection of a shear stress of 2 dynes/cm^2, representative of shear stresses found both in normal and cancerous [63–65] (1–30 dynes/cm^2) as well as embryonic [66] (0–5.5 dynes/cm^2) tissues, resulted in low microbubble attachment numbers (<1 MB/cell). Nevertheless, our results demonstrated that MB_E binding was approximately twofold higher in $Eng^{+/+}$ cells ($Eng^{+/+}_{median} = 0.96$ MB_E/cell) compared with heterozygous cells ($Eng^{+/-}_{median} = 0.40$ MB_E/cell) and fivefold higher than endoglin null cells ($Eng^{-/-}_{median} = 0.19$ MB_E/cell). This finding strongly

suggests that microbubble accumulation in vitro is proportional to receptor density on endothelial cells, as we were able to achieve elevated levels of MB_E binding compared with MB_C and MB_U across genotypes, except in the case of MB_C attachment to $Eng^{+/-}$ cells. We speculate that reductions in endoglin levels may affect the cell morphology or presence of various surface receptors in a way that encourages non-specific or Fc binding in a manner that differs from endoglin null cells, which do not display this phenotype. Elevated levels of MB_C binding did not translate in vivo, highlighting the challenge of working with suitable microbubble binding models and the need for corroborative binding evidence in in vivo model systems.

In a few instances, we observed microbubbles bound in groups, making it difficult to distinguish individual bubbles. For the very smallest bubbles, it was not always possible to differentiate between a bound and potentially free-floating microbubble. However, since endoglin expression varies across cells of the same genotype, it was necessary to balance taking representative images of the entire cell population with resolution of all bubbles. In future studies, it may be possible to assess targeted binding at the individual cell level by correlating microbubble adherence with a measure of individual cell expression, either through use of fluorescent labeling or quantitative staining. Whether this level of detail is possible or clinically beneficial cannot be assessed from this work. Our primary goal of demonstrating significant differences in in vitro targeted microbubble binding across distinct genotype populations was, however, achieved.

Finally, we expanded on previous microbubble work in murine embryos to examine whether molecular ultrasound and targeted microbubble imaging may be used to quantitatively assess endoglin expression levels. Prior studies revealed injections at stages E16.5 and E17.5 to be the most robust [26] and since endoglin expression within the brain between E15.5 and E18.5 is relatively consistent [67], we selected this as our time-point. By using isolated, living embryos, we were able to perform ultrasound imaging in a controlled and reproducible manner, without obstruction or complications from motion of the mother. Average CMPRs were acquired for each genotype and bubble type. By injecting MB_C and MB_U, we were able to establish a signal baseline in both populations against which MB_E CMPRs (significantly higher, $p < 0.001$) could be compared. MB_E enhancement levels were found to be nearly twofold higher ($p < 0.001$) in $Eng^{+/+}$ embryos ($CMPR^{+/+} = 9.71 \pm 0.66$, 95 % CI) compared to $Eng^{+/-}$ embryos ($CMPR^{+/-} = 5.51 \pm 0.64$, 95 % CI). Of the experimental parameters tested (including heart rate and injection rate), microbubble type, genotype and their interaction (microbubble type × genotype) were found to be the only significant predictors of CMPR. These in vivo results support the in vitro findings.

It is expected that changes in oxygenation and physiology will occur, although we do not anticipate these to dramatically affect microbubble performance [68]. It may, however, influence expression levels, as endoglin is upregulated under hypoxic conditions and is transcriptionally modulated by HIF-1α [32]. We also assume that the vasculature between embryonic genotypes is the same insofar as microbubble binding is concerned. Although endoglin haploinsufficiency has been shown to affect some vascular parameters [35, 69] in 129/Ola and C57BL/6 strains, these have not been characterized or observed in the CD-1 mouse. Any difference in binding signal is thus attributed to differences in endoglin expression. Furthermore, the embryos were assessed as a population, in part due to the relative (semiquantitative) nature of the Western blot, flow cytometry and targeted microbubble imaging employed here. A more detailed, quantitative examination of individual expression levels that may be directly compared to CMPRs may be necessary in validating the use of molecular ultrasound for clinical purposes. Improvement in these areas will be the focus of future endeavors. We cannot extend our measurements to the endoglin null embryo, as total inhibition of endoglin is lethal at E10.5 [23]. One alternative is to target clinically relevant biomarkers that do not present as embryonic null, such as integrins ($\alpha_2\beta_1$ [21], $\alpha_v\beta_3$ [70]) and platelet endothelial cell adhesion molecule-1 [71], as well as those involved in the process of inflammation (vascular cell adhesion molecule-1 [72], intercellular adhesion molecule-1 [73] and molecule-2 [74] and P-selectin [22]). Another option is to consider transitioning this work into an in utero model. While motion artifacts, challenges in guiding needles and complications caused by bleeding [46] are to be expected, an in utero technique would allow repeated injections of the same animal over time. This could be particularly useful for looking at response of embryos to therapeutic or blocking agents. Replication of these results in utero would be a convincing step toward clinical translation.

Combined, our in vitro and embryo results provide a concrete demonstration of the ability of contrast-enhanced molecular ultrasound to differentiate between endoglin genotypes. This is the first example to successfully relate targeted microbubble binding to differences in receptor densities in a quantitative and reproducible manner. Further work with additional model systems will be required to better understand the mechanisms involved in imaging targeted microbubble quantification (e.g., bubble adhesion and detection algorithms) and to elucidate whether more incremental changes in biomarker expression can be detected and accurately quantified. It is likely that as more vascular disease specific targets are identified, molecular imaging will play a more prominent role in the clinical evaluation of vascular therapies, increasing the need for

methods that can reliably detect and quantify disease progression and response to treatment. Quantitative correlation between target expression levels and noninvasive imaging will be a critical step toward improving our understanding of targeted microbubble binding in the context of vascular biology, paving the way for a broad spectrum of molecular ultrasound applications.

Acknowledgments The authors would like to thank John M. Hudson for assistance with microbubble handling and Valentin Sotov for assistance with MEEC Western blotting. This work was supported by the Terry Fox Programme of the National Cancer Institute of Canada.

Conflict of interest F.S. Foster acknowledges his role as consultant to VisualSonics Inc.

Ethical standard The experimental procedures performed in this study were approved by the Animal Care Committee at Sunnybrook Research Institute (Toronto, ON, Canada).

References

1. Nassiri F, Cusimano MD, Scheithauer BW et al (2011) Endoglin (CD105): a review of its role in angiogenesis and tumor diagnosis, progression and therapy. Anticancer Res 31:2283–2290
2. Deshpande N, Ren Y, Foygel K, Rosenberg J, Willmann JK (2011) Tumor angiogenic marker expression levels during tumor growth: longitudinal assessment with molecularly targeted microbubbles and US imaging. Radiology 258:804–811
3. Lindner JR (2004) Microbubbles in medical imaging: current applications and future directions. Nat Rev Drug Discov 3:527–533
4. Inaba Y, Lindner JR (2012) Molecular imaging of disease with targeted contrast ultrasound imaging. Transl Res 159:140–148
5. Voigt JU (2009) Ultrasound molecular imaging. Methods 48:92–97
6. Klibanov A (2009) Preparation of targeted microbubbles: ultrasound contrast agents for molecular imaging. Med Biol Eng Comput 47:875–882
7. Pysz MA, Foygel K, Rosenberg J, Gambhir SS, Schneider M, Willmann JK (2010) Antiangiogenic cancer therapy: monitoring with molecular US and a clinically translatable contrast agent (BR55). Radiology 256:519–527
8. Palmowski M, Huppert J, Ladewig G et al (2008) Molecular profiling of angiogenesis with targeted ultrasound imaging: early assessment of antiangiogenic therapy effects. Mol Cancer Ther 7:101–109
9. Weller GER, Villanueva FS, Klibanov AL, Wagner WR (2002) Modulating targeted adhesion of an ultrasound contrast agent to dysfunctional endothelium. Ann Biomed Eng 30:1012–1019
10. Ferrante EA, Pickard JE, Rychak J, Klibanov A, Ley K (2009) Dual targeting improves microbubble contrast agent adhesion to VCAM-1 and P-selectin under flow. J Control Release 140:100–107
11. Garcia MD, Udan RS, Hadjantonakis AK, Dickinson ME (2011) Live imaging of mouse embryos. Cold Spring Harb Protoc 2011:pdb. top104
12. Lee DJ, Lyshchik A, Huamani J, Hallahan DE, Fleischer AC (2008) Relationship between retention of a vascular endothelial growth factor receptor 2 (VEGFR2)-targeted ultrasonographic contrast agent and the level of VEGFR2 expression in an in vivo breast cancer model. J Ultrasound Med 27:855
13. Leong-Poi H (2009) Molecular imaging using contrast-enhanced ultrasound: evaluation of angiogenesis and cell therapy. Cardiovasc Res 84:190–200
14. Cai W, Chen K, Mohamedali KA et al (2006) PET of vascular endothelial growth factor receptor expression. J Nucl Med 47:2048–2056
15. Takalkar AM, Klibanov AL, Rychak JJ, Lindner JR, Ley K (2004) Binding and detachment dynamics of microbubbles targeted to P-selectin under controlled shear flow. J Control Release 96:473–482
16. Cregger M, Berger AJ, Rimm DL (2006) Immunohistochemistry and quantitative analysis of protein expression. Arch Pathol Lab Med 130:1026–1030
17. Gassmann M, Grenacher B, Rhode B, Johannes V (2009) Quantifying Western blots: pitfalls of densitometry. Electrophoresis 30:1845
18. Moestue SA, Gribbestad IS, Hansen R (2012) Intravascular targets for molecular contrast-enhanced ultrasound imaging. Int J Mol Sci 13:6679–6697
19. Audenet F, Yates DR, Cancel-Tassin G, Cussenot O, Rouprêt M (2012) Genetic pathways involved in carcinogenesis of clear cell renal cell carcinoma: genomics towards personalized medicine. BJU Int 109:1864–1870
20. Zhang W, Ran S, Sambade M, Huang X, Thorpe PE (2002) A monoclonal antibody that blocks VEGF binding to VEGFR2 (KDR/Flk-1) inhibits vascular expression of Flk-1 and tumor growth in an orthotopic human breast cancer model. Angiogenesis 5:35–44
21. Mercurio AM (2002) Lessons from the α2 integrin knockout mouse. Am J Pathol 161:3
22. Johnson RC, Mayadas TN, Frenette PS et al (1995) Blood cell dynamics in P-selectin-deficient mice. Blood 86:1106–1114
23. Bourdeau A, Faughnan ME, Letarte M (2000) Endoglin-deficient mice, a unique model to study hereditary hemorrhagic telangiectasia. Trends Cardiovasc Med 10:279–285
24. Aristizábal O, Williamson R, Turnbull DH (2007) 12A-4 In vivo 3D contrast-enhanced imaging of the embryonic mouse vasculature. In: Ultrasonics Symposium, 2007, IEEE, New York, pp 1073–1076
25. Bartelle BB, Berríos-Otero CA, Rodriguez JJ, Friendland AE, Aristizábal O, Turnbull DH (2012) Novel genetic approach for in vivo vascular imaging in mice. Circ Res 110:938–947
26. Denbeigh JM, Nixon BA, Hudson JM, Purin MC, Foster FS (2014) VEGFR2-targeted molecular imaging in the mouse embryo: an alternative to the tumor model. Ultrasound Med Biol 40:389–399
27. Quackenbush EJ, Letarte M (1985) Identification of several cell surface proteins of non-T, non-B acute lymphoblastic leukemia by using monoclonal antibodies. J Immunol 134:1276–1285
28. Paauwe M, ten Dijke P, Hawinkels LJAC (2013) Endoglin for tumor imaging and targeted cancer therapy. Expert Opin Ther Targets 17:421–435
29. Cheifetz S, Bellón T, Calés C et al (1992) Endoglin is a component of the transforming growth factor-beta receptor system in human endothelial cells. J Biol Chem 267:19027–19030
30. Nomura-Kitabayashi A, Anderson GA, Sleep G et al (2009) Endoglin is dispensable for angiogenesis, but required for endocardial cushion formation in the midgestation mouse embryo. Dev Biol 335:66–77
31. Dallas NA, Samuel S, Via L et al (2008) Endoglin (CD105): a marker of tumor vasculature and potential target for therapy. Clin Cancer Res 14:1931–1937
32. Sánchez-Elsner T, Botella LM, Velasco B, Langa C, Bernabéu C (2002) Endoglin expression is regulated by transcriptional

cooperation between the hypoxia and transforming growth factor-beta pathways. J Biol Chem 277:43799–43808
33. McAllister KA, Grogg KM, Johnson DW et al (1994) Endoglin, a TGF-β binding protein of endothelial cells, is the gene for hereditary haemorrhagic telangiectasia type 1. Nat Genet 8:345–351
34. Venkatesha S, Toporsian M, Lam C et al (2006) Soluble endoglin contributes to the pathogenesis of preeclampsia. Nat Med 12:642–649
35. ten Dijke P, Goumans MJ, Pardali E (2008) Endoglin in angiogenesis and vascular diseases. Angiogenesis 11:79–89
36. Korpanty G, Grayburn PA, Shohet RV, Brekken RA (2005) Targeting vascular endothelium with avidin microbubbles. Ultrasound Med Biol 31:1279–1283
37. Korpanty G, Carbon JG, Grayburn PA, Fleming JB, Brekken RA (2007) Monitoring response to anticancer therapy by targeting microbubbles to tumor vasculature. Clin Cancer Res 13:323–330
38. Zhang Y, Yang Y, Hong H, Cai W (2011) Multimodality molecular imaging of CD105 (Endoglin) expression. Int J Clin Exp Med 4:32
39. Dales JP, Garcia S, Carpentier S et al (2004) Long-term prognostic significance of neoangiogenesis in breast carcinomas: comparison of Tie-2/Tek, CD105, and CD31 immunocytochemical expression. Hum Pathol 35:176–183
40. Pece-Barbara N, Vera S, Kathirkamathamby K et al (2005) Endoglin null endothelial cells proliferate faster and are more responsive to transforming growth factor β1 with higher affinity receptors and an activated Alk1 pathway. J Biol Chem 280:27800–27808
41. Jerkic M, Rivas-Elena JV, Prieto M et al (2004) Endoglin regulates nitric oxide-dependent vasodilatation. FASEB J 18:609–611
42. Willmann JK, Kimura RH, Deshpande N, Lutz AM, Cochran JR, Gambhir SS (2010) Targeted contrast-enhanced ultrasound imaging of tumor angiogenesis with contrast microbubbles conjugated to integrin-binding knottin peptides. J Nucl Med 51:433–440
43. Whiteley KJ, Adamson SL, Pfarrer CD (2006) Vascular corrosion casting of the uteroplacental and fetoplacental vasculature in mice. In: Soares MJ, Hunt JS (eds) Placenta and trophoblast: methods and protocols. Humana Press, Totowa, pp 371–392
44. Lyshchik A, Fleischer AC, Huamani J, Hallahan DE, Brissova M, Gore JC (2007) Molecular imaging of vascular endothelial growth factor receptor 2 expression using targeted contrast-enhanced high-frequency ultrasonography. J Ultrasound Med 26:1575–1586
45. Jerkic M, Rodriguez-Barbero A, Prieto M et al (2006) Reduced angiogenic responses in adult Endoglin heterozygous mice. Cardiovasc Res 69:845–854
46. Yamada M, Hatta T, Otani H (2008) Mouse exo utero development system: protocol and troubleshooting. Congenit Anom 48:183–187
47. Kaufmann BA, Sanders JM, Davis C et al (2007) Molecular imaging of inflammation in atherosclerosis with targeted ultrasound detection of vascular cell adhesion molecule-1. Circulation 116:276–284
48. Barreiro O, Aguilar RJ, Tejera E et al (2009) Specific targeting of human inflamed endothelium and in situ vascular tissue transfection by the use of ultrasound contrast agents. JACC Cardiovasc Imaging 2:997–1005
49. Pochon S, Tardy I, Bussat P et al (2010) BR55: a lipopeptide-based VEGFR2-targeted ultrasound contrast agent for molecular imaging of angiogenesis. Invest Radiol 45:89–95
50. Dayton PA, Rychak JJ (2007) Molecular ultrasound imaging using microbubble contrast agents. Front Biosci 12:5124–5142
51. Gessner R, Dayton PA (2010) Advances in molecular imaging with ultrasound. Mol Imaging 9:117–127
52. Unnikrishnan S, Klibanov AL (2012) Microbubbles as ultrasound contrast agents for molecular imaging: preparation and application. Am J Roentgenol 199:292–299
53. Williams R, Hudson JM, Lloyd BA et al (2011) Dynamic microbubble contrast-enhanced US to measure tumor response to targeted therapy: a proposed clinical protocol with results from renal cell carcinoma patients receiving antiangiogenic therapy. Radiology 260:581
54. Cai W, Chen X (2008) Multimodality molecular imaging of tumor angiogenesis. J Nucl Med 49:113S–128S
55. Saini R, Sorace AG, Warram JM, Mahoney MJ, Zinn KR, Hoyt K (2013) an animal model allowing controlled receptor expression for molecular ultrasound imaging. Ultrasound Med Biol 39:172–180
56. Toporsian M, Gros R, Kabir MG et al (2005) A role for endoglin in coupling eNOS activity and regulating vascular tone revealed in hereditary hemorrhagic telangiectasia. Circ Res 96:684–692
57. Wu J, Leong-Poi H, Bin J et al (2011) efficacy of contrast-enhanced US and magnetic microbubbles targeted to vascular cell adhesion molecule-1 for molecular imaging of atherosclerosis. Radiology 260:463
58. Guenther F, von zur Muhlen C, Ferrante EA, Grundmann S, Bode C, Klibanov AL (2010) An ultrasound contrast agent targeted to p-selectin detects activated platelets at supra-arterial shear flow conditions. Invest Radiol 45:586
59. Rychak JJ, Lindner JR, Ley K, Klibanov AL (2006) Deformable gas-filled microbubbles targeted to P-selectin. J Control Rel 114:288–299
60. Bachmann C, Klibanov AL, Olson TS et al (2006) Targeting mucosal addressin cellular adhesion molecule (MAdCAM)-1 to noninvasively image experimental Crohn's disease. Gastroenterology 130:8
61. Anderson CR, Rychak JJ, Backer M, Backer J, Ley K, Klibanov AL (2010) scVEGF microbubble ultrasound contrast agents: a novel probe for ultrasound molecular imaging of tumor angiogenesis. Invest Radiol 45:579
62. Phillips LC, Klibanov AL, Wamhoff BR, Hossack JA (2012) Intravascular ultrasound detection and delivery of molecularly targeted microbubbles for gene delivery. IEEE Trans Ultrason Ferroelectr Freq Control 59:1596–1601
63. Wirtz D, Konstantopoulos K, Searson PC (2011) The physics of cancer: the role of physical interactions and mechanical forces in metastasis. Nat Rev Cancer 11:512–522
64. Buchanan CF, Voigt EE, Szot CS, Freeman JW, Vlachos PP, Rylander MN (2013) Three-Dimensional microfluidic collagen hydrogels for investigating flow-mediated tumor-endothelial signaling and vascular organization. Tissue Eng C Methods 20(1):64–75
65. Monsky WL, Carreira CM, Tsuzuki Y, Gohongi T, Fukumura D, Jain RK (2002) Role of host microenvironment in angiogenesis and microvascular functions in human breast cancer xenografts: mammary fat pad vs cranial tumors. Clin Cancer Res 8:1008–1013
66. Jones EAV, Baron MH, Fraser SE, Dickinson ME (2004) Measuring hemodynamic changes during mammalian development. Am J Physiol Heart Circ Physiol 287:H1561–H1569
67. Allen Institute for Brain Science (2013) Allen developing mouse brain atlas: endoglin gene. http://developingmouse.brain-map.org
68. Mullin L, Gessner R, Kwan J, Kaya M, Borden MA, Dayton PA (2011) Effect of anesthesia carrier gas on in vivo circulation times of ultrasound microbubble contrast agents in rats. Contrast Media Mol Imaging 6:126–131
69. Aird WC (2007) Endothelial biomedicine. Cambridge University Press, New York
70. Hodivala-Dilke K (2008) αvβ3 integrin and angiogenesis: a moody integrin in a changing environment. Curr Opin Cell Biol 20:514–519

71. Duncan GS, Andrew DP, Takimoto H et al (1999) Genetic evidence for functional redundancy of platelet/endothelial cell adhesion molecule-1 (PECAM-1): CD31-deficient mice reveal PECAM-1-dependent and PECAM-1-independent functions. J Immunol 162:3022–3030
72. Cybulsky MI, Iiyama K, Li H et al (2001) A major role for VCAM-1, but not ICAM-1, in early atherosclerosis. J Clin Invest 107:1255–1262
73. Xu H, Gonzalo JA, St Pierre Y et al (1994) Leukocytosis and resistance to septic shock in intercellular adhesion molecule 1-deficient mice. J Exp Med 180:95–109
74. Gerwin N, Gonzalo JA, Lloyd C et al (1999) Prolonged eosinophil accumulation in allergic lung interstitium of ICAM-2-deficient mice results in extended hyperresponsiveness. Immunity 10:9–19